



ELSEVIER

Palaeogeography, Palaeoclimatology, Palaeoecology 200 (2003) 163–185

PALAEO

www.elsevier.com/locate/palaeo

Stratigraphic modelling of carbonate platform-to-basin sediments (Maastrichtian to Paleocene) in the Eastern Desert, Egypt

C. Scheibner*, J. Kuss, R.P. Speijer

Universität Bremen, FB5, P.O.Box 330440, 28334 Bremen, Germany

Received 28 September 2001; accepted 21 March 2003

Abstract

In the Galala Mountains of the Eastern Desert, Egypt, carbonate platform and basin deposits have excellent exposure. These exposures show a late Campanian–early Paleocene rimmed platform evolving into a late Paleocene distally steepened ramp. We modelled the evolution of the platform–basin transition from the Maastrichtian to Selandian (68.7–59 Ma) with the 2-D stratigraphic simulation program PHIL and compared the modelled results with outcrop sections. Stratigraphic, facies, and environmental data are summarized and operate as input and control parameters for the computer simulation. The most important parameters that control the depositional geometries of the late Cretaceous mixed carbonate siliciclastic platform and the Paleogene carbonate platform are changes in relative sea level, sediment flux and initial topography. The simulation provides an understanding of platform growth and slope to basin deposition, particularly in areas of the platform that are poorly exposed or have been eroded. Moreover, the simulated geologic parameters like lithology, overall thickness and palaeowater depth closely resemble field and laboratory measurements of the individual sections. In an earlier study, the Maastrichtian slope angle was calculated to be 5–8° and this was confirmed in this study. In this earlier study also the timing of the transition from a rimmed platform to a distally steepened ramp was established to be during latest Maastrichtian–early Paleocene. The present study shows that the rimmed platform persisted at least until the late Paleocene (59 Ma), as indicated by the relatively high slope angle of 6°.

© 2003 Elsevier B.V. All rights reserved.

Keywords: Galala Mountains; Egypt; Maastrichtian; Paleocene; sedimentation rates; stratigraphic modelling; platform–basin transition

1. Introduction

The area of the Galala Mountains (Eastern Desert, Egypt; Fig. 1) has been the focus of numerous studies, mostly dealing with its biostratigraphy and lithostratigraphy (e.g. Abdel Kireem and Abdou, 1979; Strougo et al., 1992; Strougo

* Corresponding author. Present address: Institut für Geowissenschaften, Universität Potsdam, Postfach 601553, 14415 Potsdam, Germany. Tel.: +49-331-9775071, Fax: +49-331-9775060.

E-mail addresses: scheibner@geo.uni-potsdam.de (C. Scheibner), kuss@uni-bremen.de (J. Kuss), speijer@uni-bremen.de (R.P. Speijer).

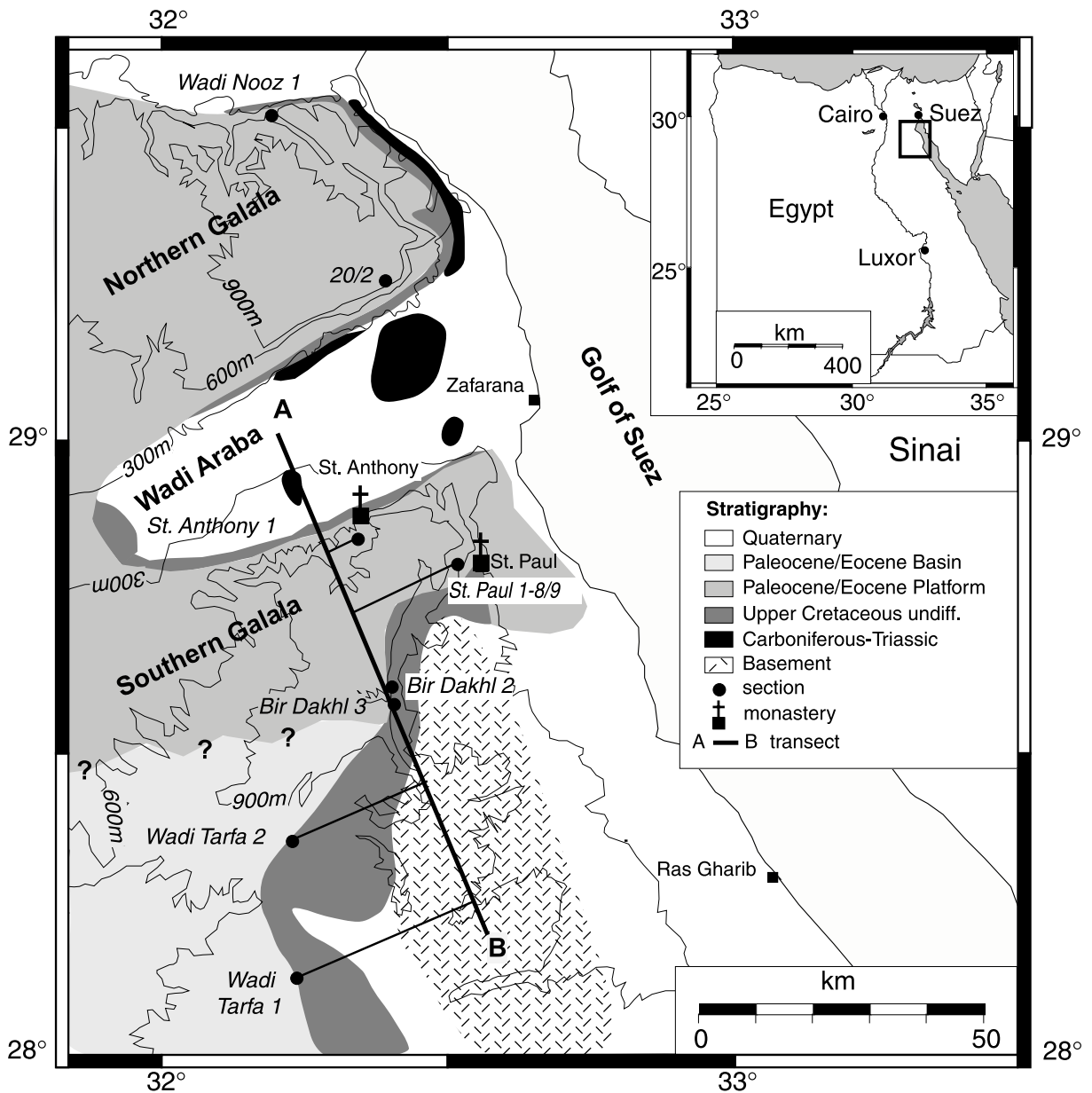


Fig. 1. Schematic geological map of the Galala Mountains in the Eastern Desert, west of the Gulf of Suez (see upper inset) with locations of sections projected on line A–B which runs in NNW–SSE direction, perpendicular to the NGWA High. The zero point of profile line A–B lies within the Wadi Araba. Sections 20/2 and Wadi Nooz 1 in the Northern Galala are only used for bio- and lithostratigraphic comparisons and not for the stratigraphic simulation. The exact stratigraphic range of the individual formations is indicated in Fig. 2.

and Faris, 1993; Faris, 1995). These studies mainly concentrated on the Upper Cretaceous and Paleogene sediments. Others dealt with the overall architecture of the depositional system

(Bandel and Kuss, 1987; Kuss and Leppig, 1989; Kulbrok, 1996; Gietl, 1998; Kuss et al., 2000; Scheibner et al., 2001a). The latter authors assumed a carbonate platform depositional sys-

tem evolving on a Syrian Arc high with a generally southward progradation direction starting in Campanian times. Recently, studies dealing with individual biosedimentary processes and their controlling parameters for this platform were initiated, suggesting for instance Maastrichtian slope angles of 5–8° (Scheibner et al., 2000, 2001b).

In this study, we concentrate on two stratigraphic computer simulations of depositional sequences and their lithologic properties for the late Maastrichtian and the early to mid-late Paleocene. The first part of this paper documents the geological data including stratigraphy, depositional setting, slope architecture, palaeobathymetry, sedimentation rates and sea-level changes. The interpretation of the extremely variable sedimentation rates receives special emphasis. In the second part the forward modelling computer program PHIL is used to simulate the depositional sequences and the lithostratigraphic properties of the time interval 68.7–59 Ma (late Maastrichtian–Selandian). A portion of the geological data serves as input data while another portion acts as a control data set for the simulation results.

The purposes of this study are: (1) to reconstruct the depositional history of the platform–basin transect in the Galala Mountains, (2) to obtain information on areas of the carbonate platform that are not or only poorly exposed, (3) to provide general insights into the processes and factors controlling the growth of carbonate platforms, (4) to test the usefulness of the computer program PHIL, and (5) to evaluate the benefits of stratigraphic modelling.

2. Geological setting

The investigated area represents a segment of the northern passive margin of the Afro–Arabian plate, formed during the late Triassic–Jurassic opening of the Neotethys with the activation of half-grabens. Beginning with the initial stages of the collision between the African and European plates during Turonian times, a dextral transpressive reactivation of the half-grabens took place along the North African–Arabian plate boundary

(e.g. Moustafa and Khalil, 1995). As a consequence, a system of inverted, uplifted and folded grabens was formed, called the Syrian Arc System (Krenkel, 1925). In Egypt this area is also known as the ‘unstable shelf’ (Said, 1962). It contrasts with the tectonically little affected area further south (the ‘stable shelf’). While the latter is characterized by laterally rather uniform marine strata, formed on a gently north-dipping shelf, small-scale facies variations characterize the basin–swell morphologies of the unstable shelf area (Kuss et al., 2000).

The Galala Mountains in the Eastern Desert together with areas on West Sinai represent a southern branch of the Syrian Arc, called the Northern Galala/Wadi Araba High (NGWA High) (Kuss et al., 2000). Upper Cretaceous–Palaeogene carbonate platform successions prograded north and southwards from the NGWA High. During the late Campanian–Maastrichtian large masses of shallow-water sediments (carbonates, marls and siliciclastics) were shed from the NGWA High, mainly in southerly directions. These sediments accumulated on the slope of a carbonate platform evidenced at the northern rim of the Southern Galala (sections around St. Anthony; Fig. 1). Further south, at the southern rim of the Southern Galala, age equivalent basinal chalks were deposited (Scheibner et al., 2001b). We assume that during the early Paleocene the platform–basin configuration remained the same. In contrast to the small area characterized by platform and slope deposition from 68.7–59 Ma, similar late Paleocene deposits have a much wider areal distribution. From Selandian times (59 Ma) onwards the platform–basin configuration changed dramatically with a rapid southward progradation resulting from the combination of tectonic movements and a falling sea level (Scheibner et al., *in press*). The slope sediments of the late Paleocene platform are characterized by mass transport deposits like slides, slumps, and debris flows that have been investigated in detail for an upper Paleocene section (Scheibner et al., 2000). The proximal basinal sediments are characterized by calciturbidites that are absent in distal areas further south (Scheibner et al., 2001a, *in press*).



3. Materials and methods

The study area extends from the Northern Galala approximately 100 km southwards to Wadi Tarfa (Fig. 1). The following six sections are considered for the stratigraphic simulation: Section St. Anthony 1 is located along the northern rim of the Southern Galala while sections St. Paul 9, Bir Dakhil 2, 3, and Wadi Tarfa 1, 2 are located further south (Fig. 1). Additional stratigraphic data, from Kuss (1986), Bandel and Kuss (1987), Kuss and Leppig (1989), Kulbrok (1996), and Gietl (1998), have been incorporated.

Facies interpretations are based on fine scale mapping of stratigraphic sections of the carbonate platform. Microscopic studies of 181 thin-sections of the Campanian–Eocene interval are supplemented by analyses of washed residues of 533 marl samples that formed the base for a high-resolution biostratigraphic framework based on calcareous nannoplankton and planktic foraminifera. For stratigraphic modelling, the forward modelling simulation program PHIL (see below) has been used on a Macintosh G3/300 MHz computer with 320 MB RAM.

3.1. Input data

The following paragraphs document the geographical and geological data that serve as input and control parameters for the stratigraphic simulation program PHIL. More details on data, interpretation and discussion can be found in Kuss et al. (2000) and Scheibner et al. (2000, 2001a, 2001b, in press).

3.1.1. Absolute ages

From the starting age for the Maastrichtian modelling (68.7 Ma; onset of CC25b after Norris et al., 1998) to the termination age for the Paleocene modelling (59 Ma), the carbonate platform

evolved in a similar mode. Furthermore, this time frame is bracketed by a hiatus in the early Maastrichtian and a significant change in the depositional setting in the late Paleocene (Scheibner et al., 2001b, in press).

3.1.2. Location of sections

All sections that were considered to be relevant as input parameters were measured by GPS. The exact positions of these locations were projected on a line that runs perpendicular to the strike of the carbonate platform (Kuss et al., 2000). The zero point (A) of the profile line A–B is assumed in Wadi Araba, the former central part of the NGWA High (Fig. 1). The assumed position of the starting point defines in turn the relative positions of the individual sections, located at the following distances from the zero point: section St. Anthony 1/16 km; section St. Paul 9/32 km; section Bir Dakhil 2/42 km; section Bir Dakhil 3/48 km; section Wadi Tarfa 2/62 km; section Wadi Tarfa 1/82 km (Fig. 1).

3.1.3. Biostratigraphy

For modelling the Maastrichtian successions, we follow the biostratigraphic schemes of Caron (1985) for planktic foraminifera, and of Perch-Nielsen (1985) and Norris et al. (1998) for calcareous nannoplankton (CC-zones) (Fig. 2). For the Paleocene and early Eocene the biostratigraphic schemes of Berggren et al. (1995) were used for planktic foraminifera (P-zones), and of Martini (1971) and Aubry (1995) for calcareous nannoplankton (NP-zones) (Fig. 2). The calibration of planktic foraminifera and calcareous nannoplankton and the absolute ages of the biochronal and stage boundaries is from Norris et al. (1998) for the Cretaceous and from Berggren et al. (1995) for the Palaeogene. More information about the biostratigraphy of the area and the sections used in this manuscript can be found in Kuss et al.

Fig. 2. Bio- and lithostratigraphic correlation of nine measured sections arranged along a transect across the NGWA High. The broad gray band (left column) reflects the current opinion on the position of the Paleocene–Eocene boundary. The biozonations of planktic foraminifera (P-zones) and calcareous nannoplankton (NP-zones for Palaeogene and CC-zones for Maastrichtian) are listed. Black areas indicate hiatuses, due to erosion or non-deposition. Question marks indicate uncertain stratigraphic ranges. On top is a 2-D transect of the platform-to-basin architecture, where the individual sections are indicated. On the right are columns of the sequence boundaries and the sedimentation rates for the slope and basin settings.

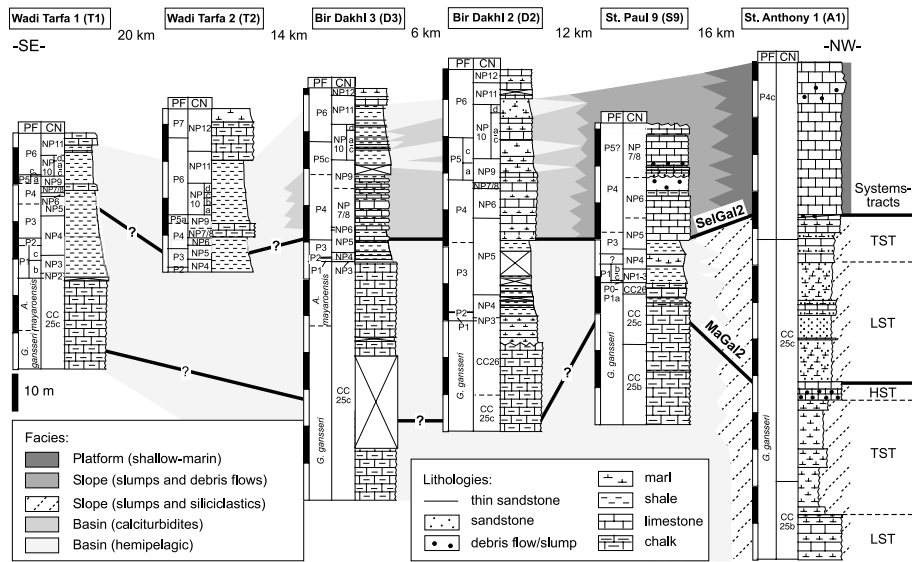


Fig. 3. Biostratigraphy and lithology of six Maastrichtian–Palaeogene sections at the Southern Galala to illustrate the field-based depositional architectures and facies variations. Best visible is the progradation of the carbonate platform in the Paleocene–Eocene. At left in the sections the biozones of planktic foraminifera (PF) and calcareous nannoplankton (CN) are plotted. The heavy black lines mark the sequence boundaries MaGal1 and SelGal2.

(2000), Scheibner et al. (2000, 2001a, 2001b), and Marzouk and Scheibner (in press).

3.1.4. Lithostratigraphy, depositional setting and lateral transitions

The Campanian–Eocene sediments of the Galala area can be subdivided into three different environmental regimes of deposition or non-deposition/erosion which remained approximately in the same geographic position (Fig. 2; Scheibner et al., 2001a). The most proximal regime is characterized by uplift and erosion or non-deposition resulting mostly from the uplift of the NGWA High structure, a branch of the Syrian Arc foldbelt. Subsequently, the shallow-water carbonate platform and slope deposits of the upper Campanian–upper Paleocene St. Anthony Formation and the upper Paleocene–lower Eocene Southern Galala Formation represent the intermediate regime and are found north and south of the NGWA High. The distal regime is represented by basinal chinks, marls and shales of the Campanian–Maastrichtian Sudr Formation and of the Paleocene–Eocene Dakhla, Tarawan, Esna Formations and the Thebes Group (Fig. 2). The distribution and lat-

eral interfingering of these formations reflect different tectonic movement, changing basin morphology, sea-level change and progradation of shallow-water sediment (Scheibner et al., 2001a).

Shallow-water carbonates and quartz-rich marls were deposited during the Cretaceous part of the St. Anthony Formation whereas phosphatic, quartz-rich marls accumulated during its Paleocene part. These sediments are exposed only in an east–west trending belt at the northern rim of the Southern Galala. Simultaneously, basinal chinks and marls of the Sudr and Dakhla Formations accumulated 14 km to the south at St. Paul (Fig. 3). The interfingering between the St. Anthony Formation and the basinal Sudr and Dakhla Formations is not exposed.

A combination of a sea-level drop and tectonic uplift in the late Paleocene (59 Ma) resulted in the prominent progradation of the carbonate platform (Scheibner et al., in press). On the distal platform patch reefs, reef debris and lagoonal to margin/upper slope limestones were deposited (section A1), whereas slumps and debris flows were stored on the steeper slope (section S9). In the basinal areas mass flow deposits transferred

into calciturbidites (sections D2, D3). Further south only basinal marls were deposited (sections T1, T2) (Scheibner et al., in press).

3.1.5. Slope architecture

Scheibner et al. (2001b) calculated the slope geometries of the late Maastrichtian (CC25) carbonate platform margin of the Galala Mountains. The initial structural topography and sedimentary patterns suggest an asymmetrical platform. This asymmetrical platform margin was rimmed in southeasterly direction while ramped in southwesterly direction. The rimmed platform is subdivided into a gentle upper slope and a steep lower slope with slope angles of the rimmed part being 5–8°, whereas the ramped part had an angle of less than 0.1°. The relatively steep slope explains the narrow depositional belt of Campanian to Maastrichtian carbonate platform–slope sediments. For the Paleocene no such detailed calculations exist but from investigations of the depositional settings a gentler inclined slope is assumed (Kulbrok, 1996; Kuss et al., 2000) which fits well with a much broader depositional belt of the Paleocene slope deposits. The slope geometries have been calculated with the aid of depth estimates based on benthic foraminiferal assemblages.

3.1.6. Paleobathymetry

The chalky and marly hemipelagic sediments deposited in the area of St. Paul's monastery and further southwards yield rich and diverse foraminiferal assemblages. These are dominated by planktic foraminifera indicating open marine conditions and good connections to the Tethys Ocean. Analysis of benthic foraminiferal assemblages is widely used as a powerful tool to estimate depositional depths (e.g. Culver, 1993). In the study area, we observed Maastrichtian and Paleocene assemblages that have previously been described from Israel, Sinai, and northern Tunisia (e.g. Reiss, 1952; Said and Kenawy, 1956; Speijer and Van der Zwaan, 1996; Widmark and Speijer, 1997b). Maastrichtian and Paleocene assemblages have a significant component of typical neritic taxa in common. This component is characterized by various species of *Anomalinoidea*, *Bulimina*, *Lenticulina*, and *Cibicidoides*, i.e. taxa that are

generally abundant in the neritic deposits of central Egypt (e.g. LeRoy, 1953; Luger, 1985; Speijer and Van der Zwaan, 1996; Speijer and Schmitz, 1998; Schnack, 2000). Another large component constituting Maastrichtian and Paleocene benthic foraminiferal assemblages is composed of various bathyal and deep-sea species. Typical Maastrichtian representatives of this are *Eouwigerina sub-sculptura*, *Slitertia varsoviensis*, *Bolivinoidea draco*, and *Sitella* spp., which all became extinct in the earliest Paleocene (Speijer and Van der Zwaan, 1996; Widmark and Speijer, 1997a; Widmark, 2000; Alegret and Thomas, 2001). In the Paleocene of Northern Egypt these taxa with deep water affinity were replaced by other typical deep-sea taxa, known as Velasco type taxa, like *Gavelinella beccariiiformis*, the most abundant one, *Gyroidinoidea globosus*, *Pullenia coryelli*, *Cibicidoides hyphalus*, *Bulimina trinitatensis*, and *Nuttallides truempyi* (e.g. Van Morkhoven et al., 1986, and references therein). The combination of typical deep-sea taxa co-occurring with shelf taxa and the similarity with foraminiferal faunas from Sinai, Israel, and northern Tunisia indicates deposition at depths of 300–500 m during the Maastrichtian, deepening to 400–600 m during the early Paleocene. We could observe no obvious down-slope differences in the benthic assemblages between St. Paul's and Wadi Tarfa, the reason for this being that the bathymetric extent of the biofacial units at these depths is supposed to have been much larger than those in neritic environments.

3.1.7. Sedimentation rates

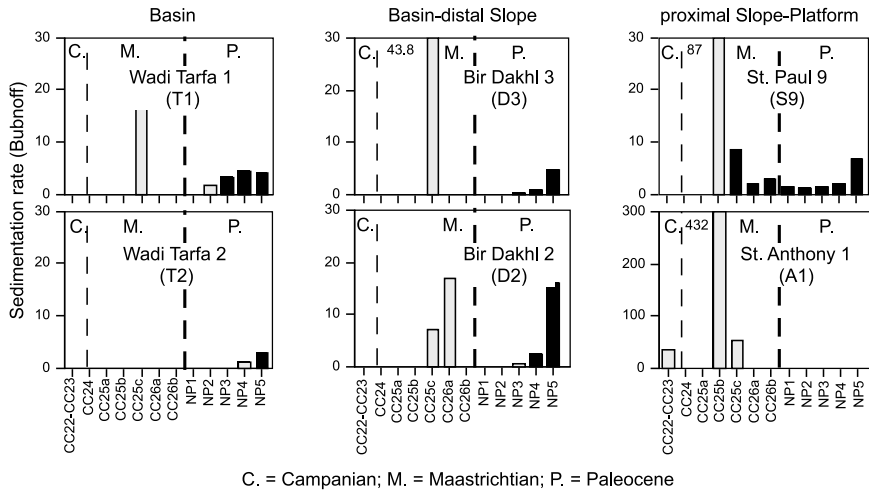
The late Cretaceous–Paleogene sedimentation rates of the Galala Mountains and adjacent areas show a high variability within the different depositional settings and time slices, and are therefore presented in detail.

The sedimentation rates are calculated for seven time intervals (CC22–CC26b) for the Campanian–Maastrichtian and five time intervals (NP1–NP5) for the Paleocene for two basinal sections, two basinal–distal slope sections and two proximal slope–platform sections (Fig. 4).

To calculate the duration of the individual biozones we used the timescale of Norris et al.

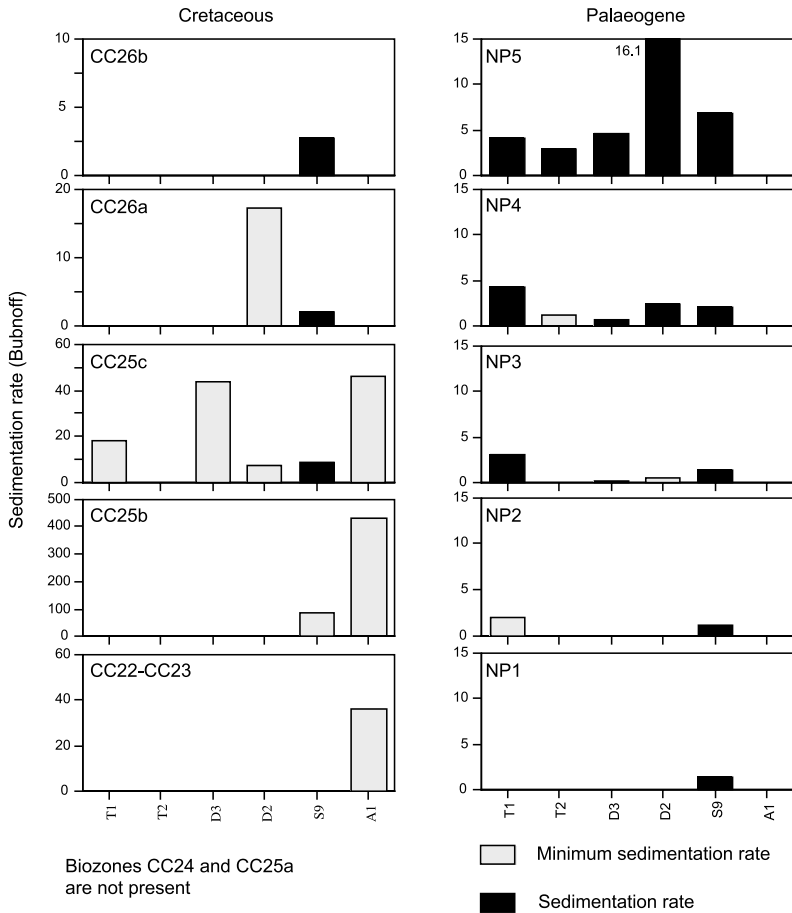
A

Sedimentation rates (sections)



B

Sedimentation rates (biozones)



(1998). Sedimentation rates are considered true sedimentation rates, if both the bottom and the top of a stratigraphic interval are marked by a biostratigraphic datum. In contrast, minimum sedimentation rates refer to stratigraphic intervals with only one or no biostratigraphic datum. All sedimentation rates are calculated for compacted sediments and are illustrated for: (1) three different depositional settings, each represented by two sections (Fig. 4A), (2) individual biozones of each section (Fig. 4B), and (3) time vs. thickness (Fig. 5a–f). Sedimentation rates are given in Bubnoffs (1 Bubnoff = 1 mm/kyr).

3.1.7.1. Cretaceous. The late Campanian–Maastriichtian sedimentation rates show the greatest variability with values ranging from 2.1 B up to 432 B (Fig. 4). Highest values are obtained in subzone CC25b both for the basinal setting (87 B in section St. Paul 9; Fig. 5b) and for the proximal slope setting (432 B in section St. Anthony 1; Fig. 5a). According to Norris et al. (1998), sub-biochron CC25b (the biostratigraphic interval between the lowest occurrence of *L. quadratus* and the lowest occurrence of *M. murus*) has a duration of 225 000 years. Either the high sedimentation rates in subzone CC25b are considered realistic or the first appearances of *L. quadratus* and/or *M. murus* are diachronous and therefore cannot be used for the absolute timescale. Diachroneity has been suggested by Norris et al. (1998) for the first appearances of *M. murus*, *N. frequens* and *M. prinsii*, but even diachroneity may not explain the extremely high values of sedimentation rates in section St. Anthony 1. These values may seem very high, but Enos (1991) compiled sedimentation rates of terrigenous shelf deposits of the North American shelf ranging from 0 to 400 B and of hemipelagic deposits ranging up to 500 B, which match the high sedimentation rates in subzone CC25b.

3.1.7.2. Paleocene. The sedimentation rates of the Paleocene range from 0.3 to 16.1 B (Fig. 4). In contrast to the higher late Cretaceous sedimentation rates, those of the early Paleocene only reach values of 4.3 B. With the onset of prograding debris flows and calciturbidites within biozone NP5 the sedimentation rates of the slope (St. Paul 9; Fig. 5b) and the mass flow influenced basinal sections (Bir Dakhl 2+3; Fig. 5c,d) show slightly higher values when compared to the basinal sections (Wadi Tarfa 1+2; Fig. 5e,f).

Recent investigations have shown that about 10 m of Lower Paleocene deposits do exist in the vicinity of St. Anthony but that the poor fossil record hampers a subdivision into biozones (Scheibner et al., in press). The average sedimentation rate for the Paleocene in this slope setting up to the initiation of the late Paleocene carbonate platform is about 1.7 B. This is very similar to the sedimentation rate of the basinal sediments for the same time.

3.1.8. Sequence stratigraphy

The modelled stratigraphic interval comprises two complete sequences, CaGal2 and MaGal1, embraced by the sequence boundaries CaGal2 and SelGal2 (Kuss et al., 2000; Scheibner et al., 2001b; Figs. 3 and 6). Sequence names are derived from a combination of the stage and the region (Galala), and relate to the underlying sequence boundaries (e.g. sequence CaGal2 is located between sequence boundary CaGal2, below, and sequence boundary MaGal1, above). The systems tracts of the sequences are best observed at the northern rim of the Southern Galala (section St. Anthony 1) where late Campanian to late Paleocene slope sediments are present (Scheibner et al., 2001b). In the sections further south chalky limestones and marls were deposited that do not allow a subdivision of sequences in systems tracts. However, the terminating sequence boundary in

Fig. 4. Sedimentation rates of six sections. The missing of values in several biozones is either due to non-deposition or hiatuses. (A) Sedimentation rates plotted against the individual biozones. Note the different scale in section St. Anthony 1. (B) Sedimentation rates of the individual biozones, plotted against different sections. Note the varying scales for the Cretaceous sedimentation rate plots.

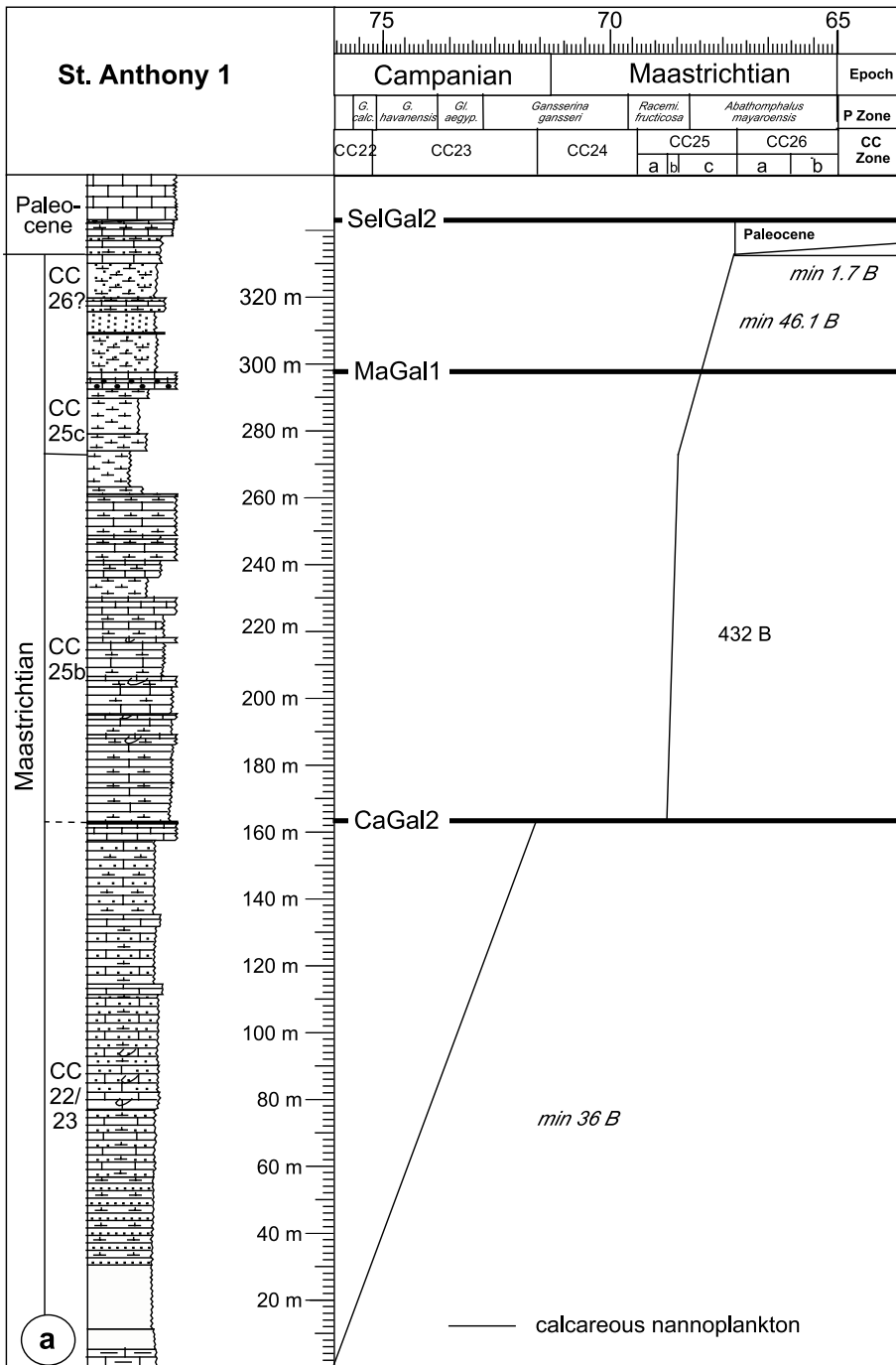


Fig. 5. Sedimentation rate plots calculated from the late Cretaceous–Palaeogene successions of six sections from the western side of the Gulf of Suez (Eastern Desert) with no correction for compaction. Note the differences in the individual plots, regarding either planktic foraminifera or calcareous nannoplankton; (all values left of the curves are for planktic foraminifera, all values right of the curves are for calcareous nannoplankton; at the bottom and at the top the values for sedimentation rates are minimum sedimentation rates). Sequence boundaries are plotted where possible. (a) St. Anthony 1. The biozonation in the upper part of the section is uncertain, but at least the last 10 m of the marl–limestone alternations belong to the Paleocene with an approximately sedimentation rate of 1.7 B up to 59 Ma.

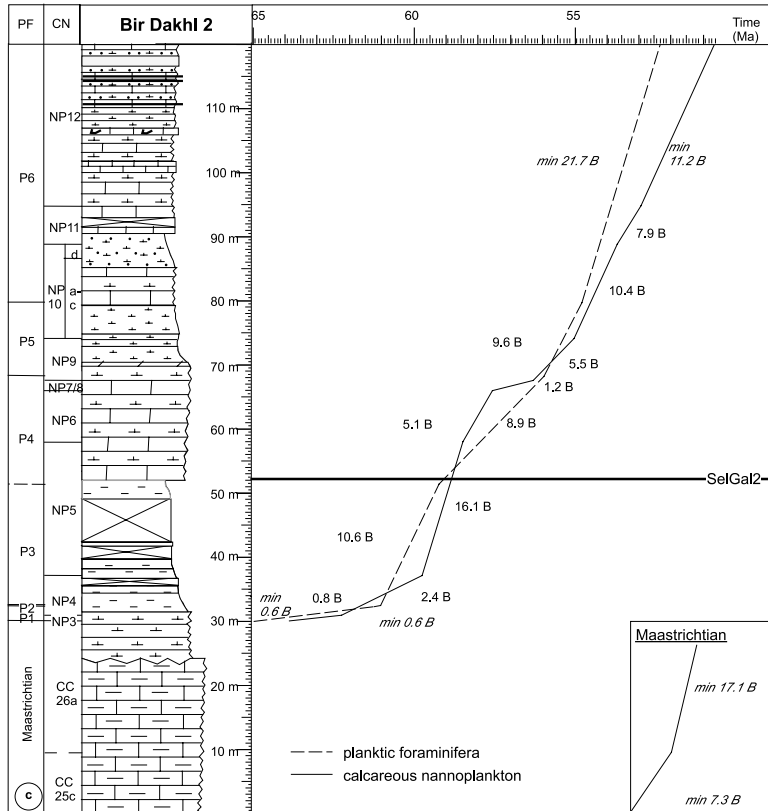
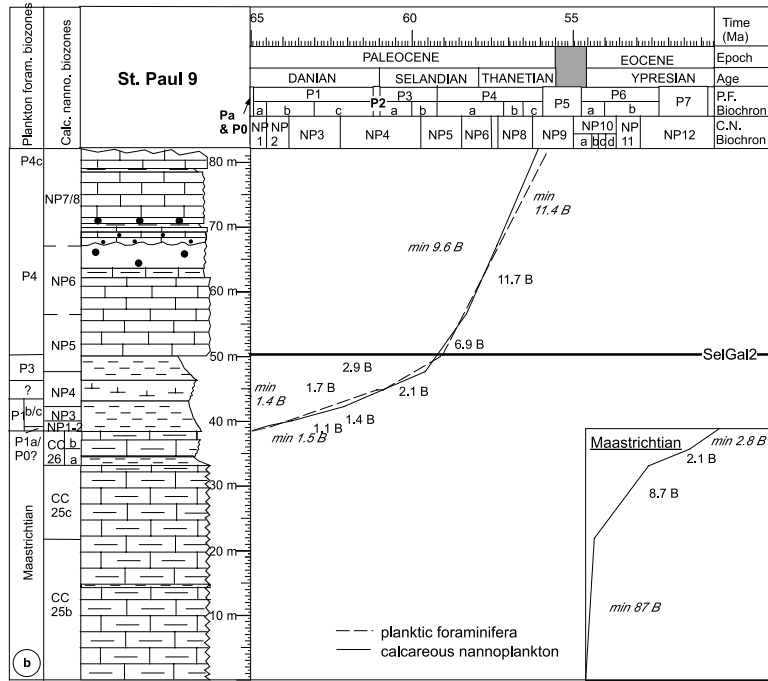


Fig. 5 (Continued).

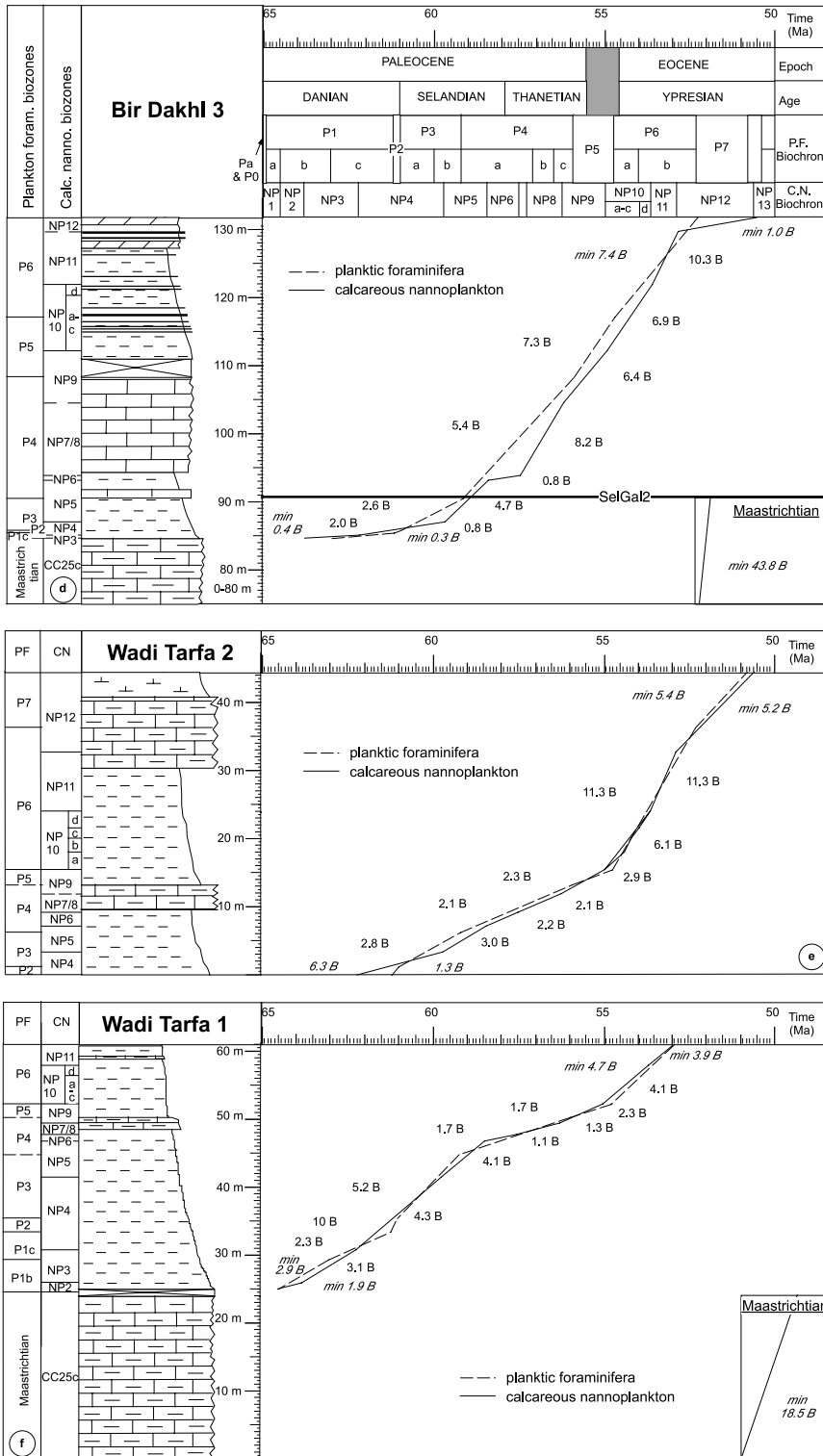


Fig. 5 (Continued).

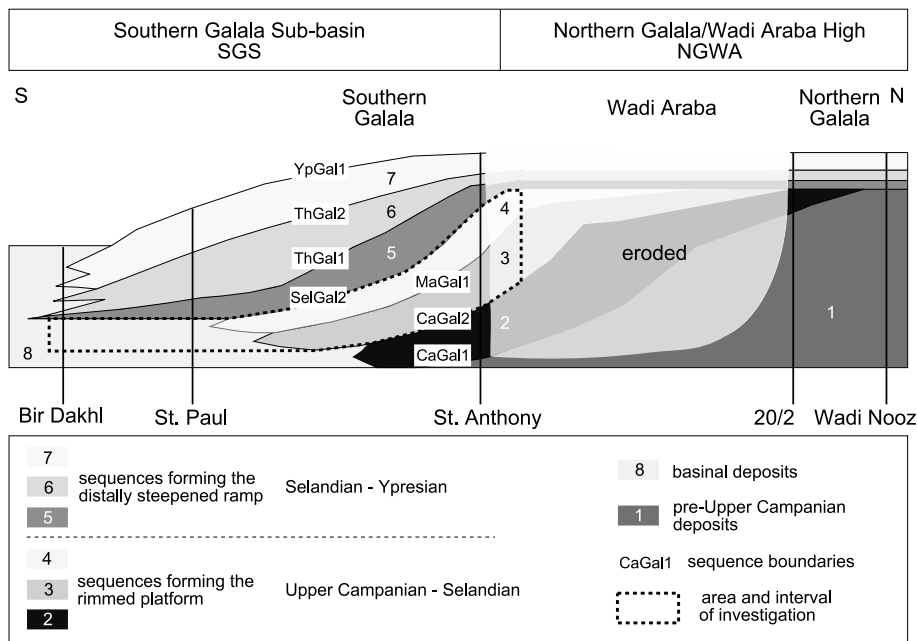


Fig. 6. Schematic cross-section for the upper Cretaceous–Paleocene sedimentary sequences to demonstrate the stratigraphic evolution of a mixed to carbonate platform at the NGWA High: (2,3,4) the rimmed carbonate platform, (4,5,6) the distally steepened ramp. Modified after Kuss et al. (2000).

this study SelGal2 is present in all depositional settings.

Sequence CaGal2: the sediments of the LST of CaGal2 are composed of marls and limestones with a subordinate siliciclastic content and exhibit conspicuous syndepositional slumpings. The TST sediments are composed of alternating hard and soft marls with relatively high planktic foraminiferal content. The overlying HST is characterized either by carbonaceous mass flow deposits or by conglomeratic, partly bedded marls to limestones with coralline algae, gastropods and echinoderms (Scheibner et al., 2001b; Fig. 3).

Sequence MaGal1: the LST sediments of MaGal1 are characterized by abundant large oysters (*Exogyra overwegi*) deposited within siliciclastic marls (Scheibner et al., 2001b). The upper part of this sequence is composed of phosphatic marls that belong to the Lower Paleocene (Scheibner et al., submitted) and represent the TST. With 9 My the duration of sequence MaGal1 is rather long and especially the Paleocene part of it is very condensed (Fig. 3).

For the modelling we used the frequency of our

sea-level curve and combined this with the amplitudes of the sea-level curve of Hardenbol et al. (1998) for the Maastrichtian. The condensed deposits in the Galala Mountains made it impossible to reconstruct a sea-level curve for the Paleocene. Therefore, we used the frequency of the Paleocene sea-level curve of Lüning et al. (1998) derived from nearby sediments on Sinai. The amplitude for the Paleocene sea-level curve was taken again from Hardenbol et al. (1998).

3.2. Stratigraphic modelling

3.2.1. General concepts

Stratigraphic computer simulation models have been developed since the late 1940s (Watney et al., 1999) for all kinds of depositional settings. For general discussions and examples of stratigraphic modelling, refer to the articles in Franseen et al. (1991) and Harbaugh et al. (1999). The main reasons for using stratigraphic computer programs to analyze sedimentary successions are: (1) the evaluation of depositional processes and their controlling parameters, and (2) the prediction of litho-

stratigraphic properties away from points of control (Perlmutter et al., 1999). The programs may help to describe depositional records that have been eroded or that are covered by younger sediments.

Modelling may be either forward or inverse. Forward models simulate sedimentary processes by using a preliminary set of input parameters. After each computer run the output is compared with the geological data set and subsequently the input parameters are modified to adjust the computer output to the real world. Inverse models, in comparison, use the structure of a forward model to simulate a specific result (Miall, 1997).

Numerous types of data are used as input parameters for computer models. Most of these parameters can be lumped into one of the following four categories: (1) accommodation, including changes in sea level and tectonics, (2) sediment supply, (3) sediment redeposition, and (4) initial depositional profile (Watney et al., 1999).

In the study presented here we use PHIL (Process-and History-Integrated Layers) as the modelling program (Marco Polo Software Inc., 1995). According to Bowman and Vail (1999), this program, which was developed by Bowman, is one of the most comprehensive models to date indicated by the inclusion of flexural loading, compaction, erosion and mass transport mechanisms. One of the major shortcomings, however, is its limitation to 2-D modelling. In recent years, PHIL has been used to model various settings in different times. For example, Read (1998) modelled ramp development and architecture during greenhouse, transitional and icehouse intervals whereas Leyrer et al. (1999) used the program to model two platform–slope–basin configurations of the Stassfurt Carbonate (Zechstein, late Permian) in Germany. Finally, Bowman and Vail (1999) modelled the history of the Baltimore Canyon Trough, offshore New Jersey, for the last 30 My.

3.2.2. *Functionality of PHIL*

The following section briefly explains the functionality of PHIL. For a detailed description and discussion refer to Bowman and Vail (1999) and Leyrer et al. (1999). The overall modelling approach of PHIL incorporates the principles employed in cellular automata. In this framework,

one of the most important assumptions is that the characteristics of each cell only depend upon the conditions in the neighboring cell (Marco Polo Software Inc., 1995). The input parameters of PHIL can be pooled into the following parameter groups (editors): spatial and time dimensions editor, basin editor, siliciclastic, carbonate and pelagic sediment editor, evaporites, organic carbon, erosion, slumping and gravity flow editor (Table 1). Within each group several single parameters can be adjusted, maintained in the default mode or deactivated. In the spatial and time dimensions editor the number of cells and time-layers used for the stratigraphic model are defined. The number of cells control the lateral resolution of the model. The chosen time-steps have to be set short enough to resolve the details of the process of interest. The best results are obtained by choosing a time increment of one half to one fourth of the shortest periodicity involved (Emery and Myers, 1996; Bowman and Vail, 1999). The basin editor allows the changing of bathymetry, water level, subsidence, compaction, flexural loading and marine currents. In the sediment editors the sedimentation rates and degrees of various depositional settings can be changed. Additionally, several input parameters can be modelled as cyclic-, time- or spatial-dependant. The results of the modelling can be displayed either as depth–distance (depth plot) or time–distance plots (chrono plot/Wheeler diagram) (Figs. 7 and 8). Furthermore, PHIL can produce stratigraphic columns for every position. For the three plot types a variety of coloured graphic displays exist, e.g. depositional systems, chronostratigraphy, lithology, systems tracts and palaeobathymetry. One major shortcoming of the simulation program PHIL is that it is a black box model so that you do not know and subsequently can not change the calculation basis. Furthermore, it is not possible to model the carbonate platform in three dimensions because of the limitation to two dimensions. Therefore we had to project all our individual sections onto one profile line (Fig. 1).

3.2.3. *Modelling procedure applied in this study*

The input parameters refer to the geologic data of this paper and interpretations from Kuss et al.

(2000) and Scheibner et al. (2000, 2001a, 2001b). They formed the first set of input data for modelling the evolution of depositional cycles in two separate simulations covering Upper Maastrichtian and Paleocene intervals. The spatial and time dimensions of the two models were specified as follows. For the Maastrichtian the starting point was defined at 68.7 Ma. This run terminated with the Cretaceous–Palaeogene boundary at 65 Ma. The Paleocene run was modelled from 65 to 59 Ma (Danian–middle Selandian). For both models the maximum spatial extension of 100 km coincided with the transect A–B (Fig. 1). The sections of St. Anthony 1, St. Paul 9, Bir Dakhl 2+3, and Wadi Tarfa 2+1 were projected onto this line and were considered reference positions from north to south. The gross depositional architecture of the study area with transitions from a rimmed plat-

form during the late Cretaceous to a distally steepened ramp during the Paleocene served as one basic input parameter to define the bottom topography. Furthermore, an angle of 8° was used as the angle of the depositional front for the Maastrichtian (Scheibner et al., 2001b) (Table 1). For the Paleocene distally steepened ramp no such calculations exist and an angle of 1.5° was assumed that was slightly higher than the angle of homoclinal ramps, according to general carbonate ramp models (Burchette and Wright, 1992). For modelling purposes sedimentation rates for each of the individual depositional settings (e.g. platform, basin) were assumed as constant through time and derived from the calculations described before. The frequency of our sea-level curve (Maastrichtian) and that of Lüning et al. (1998) (Paleocene) were incorporated into the

Table 1
The individual parameters for the Maastrichtian and Paleocene simulations with PHIL

Editor	Parameters	Maastrichtian	Paleocene	Mode
Spatial dimensions	depositional dimension	0–100 000 m	0–100 000 m	personal
	cells	500	500	personal
	cell spacing	200 m	200 m	default
	grid	0–32 000 m	0–32 000 m	personal
Time dimensions	beginning	68.7 Ma	65 Ma	personal
	final	65 Ma	59 Ma	personal
	time interval	100 000 yr	100 000 yr	personal
	layers	37	60	personal
Basin	bathymetry	personal	personal	personal
	water level	*	*	personal
	subsidence	1–5.5 m/My	default	personal/default
	compaction	over compression	over compression	default
	flexural loading	default	default	default
	marine currents	default	default	default
Siliciclastic sediment	sedimentation rate	default	switched off	default/switched off
	depositional front (°)	8°	switched off	personal/switched off
Carbonate sediment	sed. rate shelf margin	200 m/My (B)	70 m/My (B)	personal
	sed. rate shelf	130 m/My (B)	70 m/My (B)	personal
	sed. rate suspension	200 m/My (B)	40 m/My (B)	personal
	fore slope (°)	8°	6°	personal
Pelagic	sedimentation rate	15 m/My (B)	3 m/My (B)	personal
Erosion	various parameters	default	default	default
Slumping	deposition rate	default	default	default
Gravity flow	various parameters	default	default	default

In the first row the different editors of PHIL are listed, the second row names the most important parameters used in the two runs, the third and fourth rows list the individual parameters of the two runs, and in the fifth row the mode of the parameters is indicated. The asterisks in the table (water level) refer to the modified sea-level curves of Hardenbol et al. (1998) for the Maastrichtian and of Hardenbol et al. (1998) and Lüning et al. (1998) for the Paleocene (see discussion in text). Bathymetry in the basin editor is the parameter for the initial setting of the bottom topography. The sedimentation rates in PHIL are given in m/My which equates to 1 Bubnoff (B).

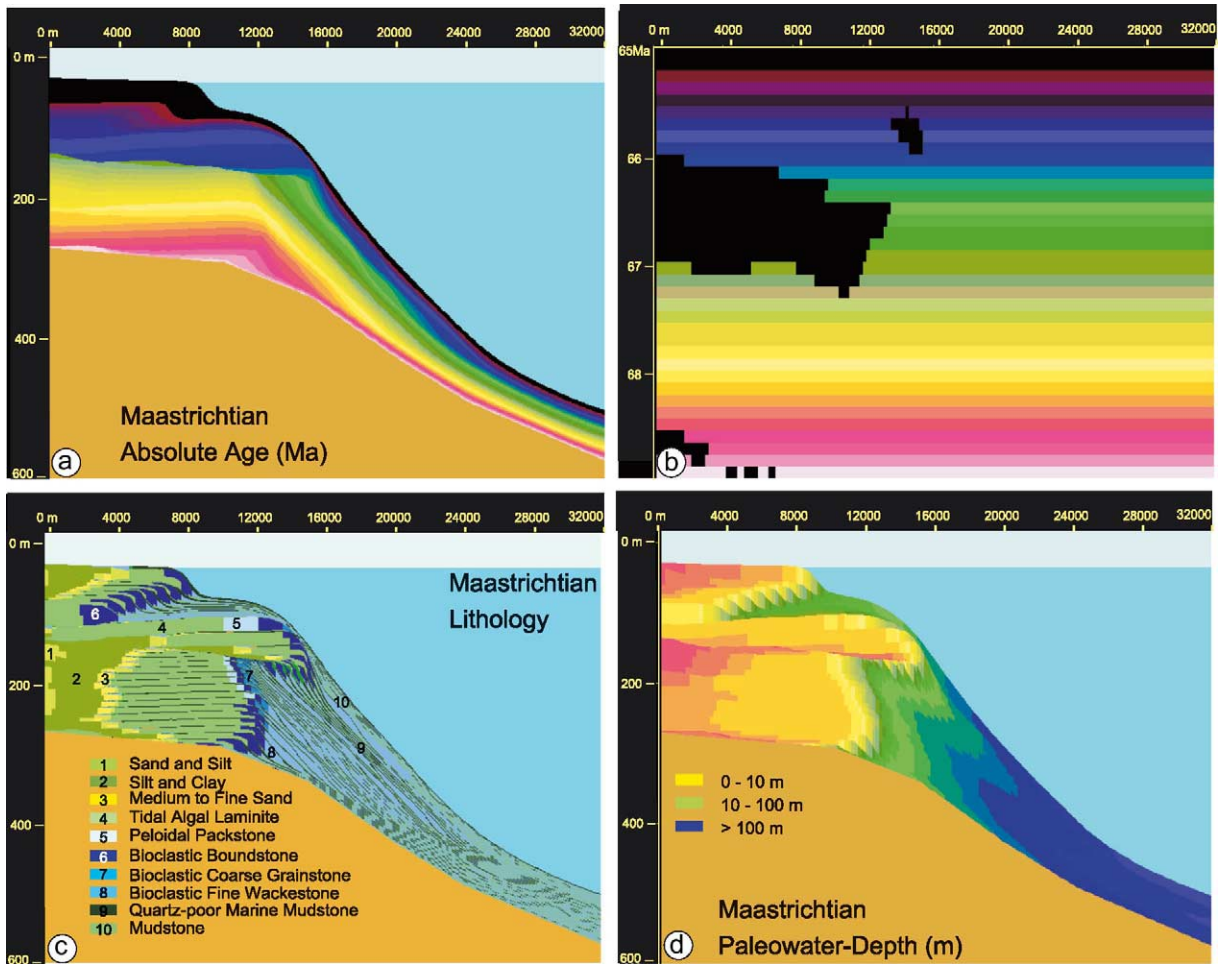


Fig. 7. Graphical display of the Late Maastrichtian (69–65 Ma) simulation results for the profile line A–B (Fig. 1). For better resolution only the first 32 km are displayed. The horizontal scales of each depth and chrono plot indicate the distance (0–32 km), while the vertical scales refer to the depth (depth plots) or to the time (chrono plot). The vertical exaggeration of the depth plots is 40 fold. (a,b) Depth plot and time plot (Wheeler diagram) of the absolute age. The colours from red to blue indicate successively younger ages with a time interval of 0.1 Ma. In the depth plot the overall thickness of the individual time slices are visible. The black colours in the time plot show the distribution of hiatuses. The large hiatus between 67 and 66 Ma in the proximal areas of the platform (0–12000 m) is due to a lowering in sea level (Fig. 9) whereas the small hiatus around 65.8 Ma is caused by an oversteepened slope and sedimentary bypass. (c) Depth plot of the lithology. The colours indicate different lithologies that are explained in the legend. On the proximal platform silt, clay, medium–fine sand and tidal algal laminites have been deposited. The shelf break is characterized by bioclastic boundstones whereas the slope is dominated by bioclastic fine wackestones and marine mud. (d) Depth plot of the palaeowater depth. From red to blue the colours indicate a deepening in palaeowater depth. During the first 2–3 Ma the platform architecture is characterized by aggradation. Around 66 Ma a tongue of shallow-water deposits is prograding to a position close to 15000 m that is followed by rapid retrogradation, which in turn is followed by another progradation. The combination of a changing sea level, sediment supply and subsidence is responsible for the change in the depositional modus.

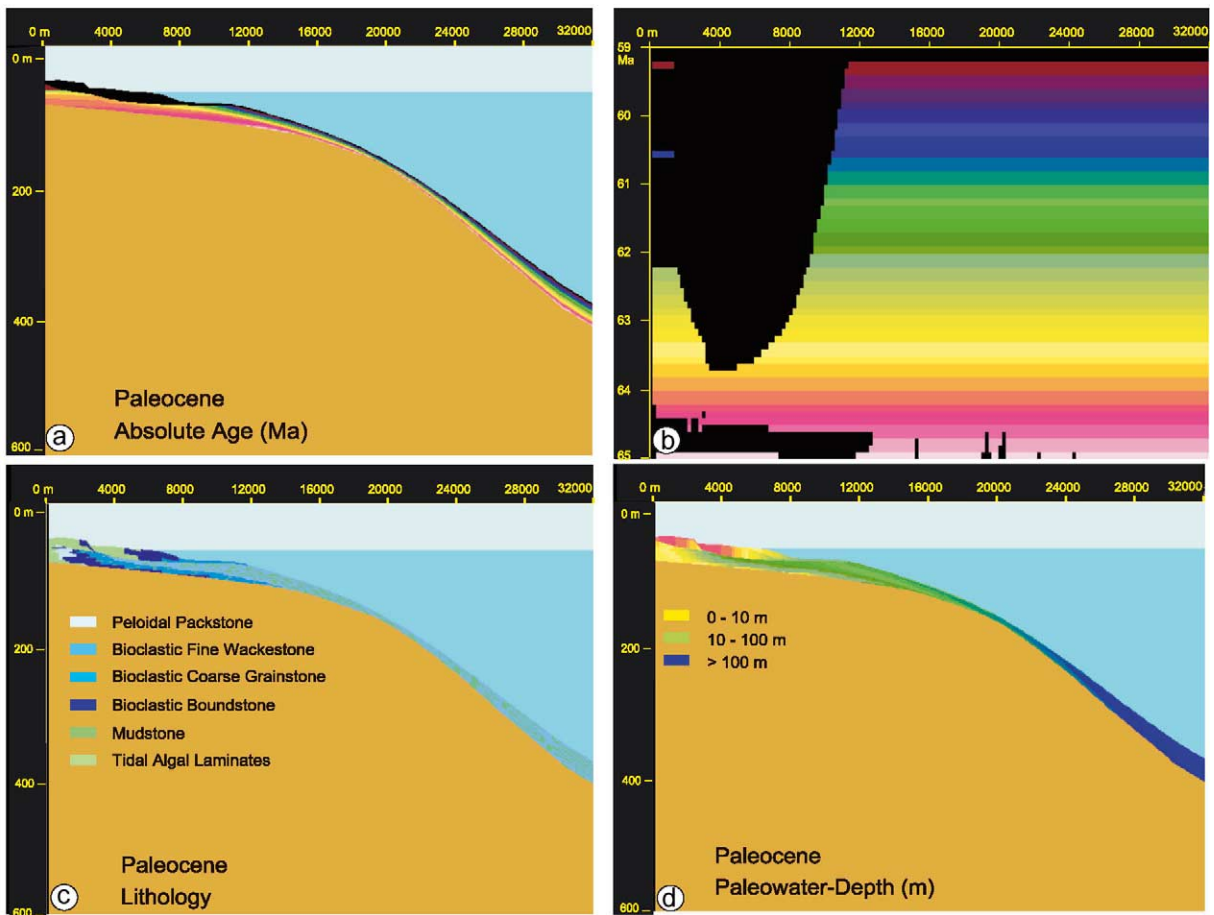


Fig. 8. Graphical display of the Paleocene (65–56 Ma) simulation results. For better resolution only the first 32 km are displayed. The horizontal scales of each depth and chrono plot indicate the distance (0–32 km), while the vertical scales refer to the depth (depth plots) or to the time (chrono plots). The vertical exaggeration of the depth plots is 40 fold. (a,b) Depth plot and time plot of the absolute age. The colours from red to blue indicate successively younger ages with a time interval of about 0.2 Ma. The black colours in the time plot show the distribution of hiatuses. (c) Depth plot of the lithology. The colours indicate different lithologies that are explained in the legend. On the proximal platform peloidal packstone and tidal algal laminates have been deposited. Siliciclastic deposits do not occur because the siliciclastic sediment editor is switched off. The shelf break is characterized by bioclastic boundstones whereas the slope is dominated by bioclastic fine wackestones and marine mud. (d) Depth plot of the palaeowater depth. From red to blue the colors indicate a deepening in palaeowater depth.

program whereas the amplitudes of the sea-level curve were derived from Hardenbol et al. (1998) for the Maastrichtian and Paleocene. The default mode was used for subsidence values for the first simulation because a subsidence analysis has not been applied to the data. Other parameters were left in the default mode or switched off, like evaporites or organic carbon that were of no interest in this study. After this basic set-up of the program, an appropriate time-step was chosen for the

first run. The output, graphic displays of various parameters, of this initial run were checked against the geologic data and the parameters were adjusted in subsequent runs, until an acceptable match was produced. Several tens of runs were necessary to produce the results presented in this study. Table 1 lists all input parameters that were used for the final simulation runs and indicates their mode (personal, default or switched off).

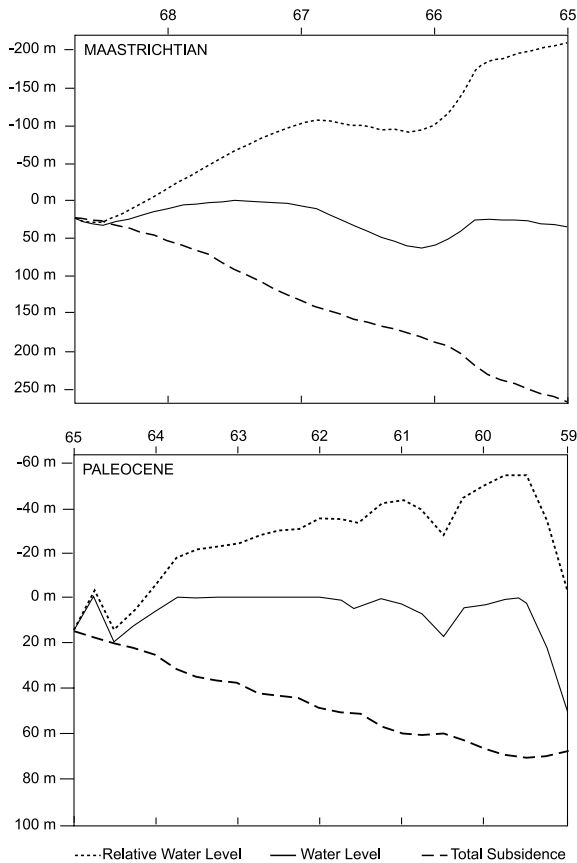


Fig. 9. Computer plots of the relative water level, the water level, and the total subsidence of the Maastrichtian (top) and the Paleocene (bottom). The combination of the total subsidence and the water level (eustatic sea level) resulted in the relative water level. The horizontal scales indicate the absolute ages, whereas the vertical scales indicate the spatial display in meters with a supposed zero level. Subsidence and lowering of sea level are positive, while uplift and rise in sea level are negative.

4. Results of the stratigraphic modelling with PHIL

For both modelled time slices the results are displayed in four different plots. The graphic output comprises three depth plots (absolute age, lithology, palaeowater depth) and 1 chrono plot (Wheeler diagram) (Figs. 7 and 8). Furthermore, the sea-level and subsidence curves are given in Fig. 9.

In Figs. 7 and 8 only the first 32 km of the totally 100-km-long transect were displayed to

emphasize the processes on the carbonate platform–slope transition. The basal areas exhibit no major changes of lithology. Therefore, only the locations of sections St. Anthony 1 at 16 km and St. Paul 9 at 32 km were visualized, whereas the more basinward sections of Bir Dakhil 2+3 and Wadi Tarfa 1+2 were neglected. Due to the different depth and distance scales a vertical exaggeration of 40 times was generated. The steepest parts of the slope have angles of 8° during the Maastrichtian and of 6° during the Paleocene.

4.1. Maastrichtian

The stratigraphic simulation of the Upper Maastrichtian covers a time interval of 3.7 My (from 68.7 to 65 Ma). More than 200 m of sediments were deposited on the carbonate platform (eroded today; Fig. 1), contrasting with only about 60 m in the basin (Fig. 7). Between 66 and 67 Ma the model predicts a hiatus on the most proximal parts of the carbonate platform with a duration of about 0.9 My (Fig. 7b). Two smaller hiatuses occur at 68.5 and 65.5 Ma. While the two older hiatuses can be attributed to a lowering of the sea level (Fig. 9), the youngest hiatus around 14 km represents a combination of rising sea-level and oversteepened slope. The slope reaches the maximum angle of 8° and, consequently, no sediments could be deposited near the platform break and were transported into the basin (Fig. 7).

The simulation predicts mainly silt and clay for the proximal platform sediments (Fig. 7c) and for the central platform areas tidal algal laminites, with minor portions of mudstones and quartz-poor marine mud. The lithology of the distal platform near the transition to the slope is simulated as bioclastic boundstones and bioclastic coarse grainstones with minor percentages of quartz-poor marine mud (Fig. 7c). During some intervals peloidal packstones dominate these environments. The sediments of the upper part of the slope are modelled as bioclastic fine wackestones with portions of mudstones and quartz-poor marine mud. Basinwards the bioclastic fine wackestones diminish and reach the same proportion as the mudstones, whereas the quartz-poor marine mud still

occurs with minor percentages. The sediment distribution on the carbonate platform is mainly controlled by variations of relative sea level (Fig. 9) and by variations of sedimentation rates within different areas of the carbonate platform (Table 1).

On the carbonate platform the palaeowater depth normally does not exceed 10 m. Only at times of a fast rising sea level the distal parts of the platform are covered by nearly 50 m of water (Fig. 7d). The palaeowater depth in the basin (at 32 km) varies around 400–500 m (Fig. 7d)

4.2. *Paleocene*

The stratigraphic simulation of the Paleocene spans an interval of 6 My (65–59 Ma). During this time interval less than 70 m of sediments are deposited on the carbonate platform, whereas in the basin thicknesses of only about 40 m occur (Fig. 8). Reasons for the reduced thicknesses (compared to the Maastrichtian) are: (1) the low sedimentation rates that affect thicknesses in both settings, and (2) long-lasting stratigraphic gaps that occur on most parts of the platform (Fig. 8b). Deposition on most parts of the carbonate platform is evidenced only for the lower Paleocene (Fig. 8a,b). The long-lasting hiatus in Lower to Upper Palaeocene is due to the oscillating relative sea paleolevel and an abrupt fall in sea level at around 59 Ma. This sea-level fall is accompanied with severe erosion on the subaerially exposed platform while sedimentation continues in the slope and basinal areas.

Field observations indicate prevailing carbonate sedimentation on the Paleocene platform with very little siliciclastic input: therefore, the modelling program runs with the siliciclastic editor switched off. The lithology on the carbonate platform is simulated as tidal algal laminites, peloidal packstones, bioclastic boundstones, and bioclastic coarse grainstones (Fig. 8c). The slope and basinal lithologies are modelled as bioclastic fine wackestones and mudstones. Sedimentation is mainly controlled by the changing relative sea level (Fig. 9).

The paleowater depth on the Palaeocene carbonate platform does not exceed 30 m, whereas

in the basin the palaeowater depth varies around 300–400 m (Fig. 8d).

4.3. *Similarities and differences of the Maastrichtian and the Paleocene models*

When comparing the plots of the Maastrichtian and Paleocene platforms, their thicknesses form the most striking discrepancy. Although the Maastrichtian platform built up during only 3.7 My, its thickness is more than double that of the Paleocene platform which was built up during 6 My. This is in agreement with the different sedimentation rates. For the Maastrichtian the maximum sedimentation rates for carbonates on the platform range between 130 and 200 B, whereas during the Paleocene they range only from 40 to 70 B (Table 1). Average sedimentation rates of the Maastrichtian pelagic setting are 15 B. This is 5 times higher than those of the Paleocene, which are only 3 B. In addition to the low Paleocene sedimentation rates, platform sediments are only preserved during the early Paleocene whereas the upper Paleocene is absent (Fig. 8b). The combination of the overall low sedimentation rates and the stratigraphic gaps leads to a reduced thickness of the Paleocene carbonate platform.

In the Maastrichtian a mixed siliciclastic–carbonate system is present (Fig. 7c,d), whereas the Paleocene platform sediments are entirely composed of carbonates (Fig. 8c). Siliciclastic lithologies dominate the proximal Maastrichtian platform and interfinger with mainly carbonate sediments of the distal platform. Apparently, the admixtures of siliciclastic sediments prohibit the formation of tidal flats and reefs. This is in agreement with the observations of Mount (1984) and Cortes and Risk (1985).

4.4. *Comparison between simulated stratigraphies and field data*

As the simulations are based in part on geologic data, both model results and field data are compared. We concentrate on the locations of the individual sections, especially the most proximal sections of St. Anthony 1 at 16 km and St. Paul 9 at 32 km, both deposited in slope to basin settings

(Figs. 7 and 8). As indicated above, the most important difference between simulation and outcrop is the absence of the carbonate platform interior due to late Cenozoic erosion (today's Wadi Araba; Fig. 1).

4.4.1. Maastrichtian

4.4.1.1. Sedimentation rates. The sedimentary sequences and the gross architecture of the upper Cretaceous platform were investigated by Kuss et al. (2000) and Scheibner et al. (2001a, 2001b). In the St. Anthony 1 section sedimentation rates are very high for subzone CC25b (Figs. 4 and 5a), whereas the younger subzones yield significantly lower sedimentation rates. A similar trend is visible in the sedimentation rates at section St. Paul 9, although here the absolute values are lower (Figs. 4 and 5b). These oscillating sedimentation rates cannot be reproduced with the set of input parameters used in the model. Instead, the sedimentary sequences are reproduced with a constant sedimentation rate through time that models the total thicknesses of the sections very well. By using constant sedimentation rates it is not possible to simulate stratigraphic gaps in areas that are not subaerially exposed. Hence, the stratigraphic gap around the K–P boundary or even smaller gaps within individual biozones are not reproducible. On the other hand, the model predicts a stratigraphic gap due to morphological reasons in the area where the oversteepened slope occurs (Fig. 7).

4.4.1.2. Slope architecture. In Scheibner et al. (2001b) a slope angle of 5–8° was calculated for the Maastrichtian rimmed platform. In our model an angle of 8° for the depositional front produces the best fit with the geological data, which is very similar to the calculated one.

4.4.1.3. Lithology. In section St. Anthony 1 the sediments of the Upper Cretaceous St. Anthony Formation are composed of chalky limestones, marls and sandstones (Scheibner et al., 2001a). At 16 km (section St. Anthony 1) the model simulates deposition of mainly bioclastic fine wackestones with minor percentages of mudstones and quartz-poor marine mud. In the basal sections

St. Paul 9 to Wadi Tarfa 1 chalk–marl couplets with thick chalk beds and thin marl beds dominate and are modelled as bioclastic fine wackestones and mudstones with minor percentages of quartz-poor marine mud.

4.4.1.4. Palaeowater depth. Scheibner et al. (2001b) assumed palaeowater depths of about 100 m for section St. Anthony 1 and of about 300–500 m for section St. Paul 9. The computer model calculated palaeowater depths of 100–150 m at 16 km (section St. Anthony 1) and of 400–500 m at 32 km (section St. Paul 9) that fit both well within the assumed range. In section St. Paul 9 (Fig. 4) a thin marly bed with an admixture of neritic benthic foraminifera was deposited that may have coincided with the lowermost drop in sea level. In the upper part of section St. Anthony 1 siliciclastic sediments with *Exogyra overwegi* occur that should have been deposited at shallower water depths (Fig. 5a). This may correlate with the drop in relative sea level around 66–67 Ma (Fig. 9). The results for modelled palaeowater depth resemble the geologic data very well.

4.4.2. Paleocene

4.4.2.1. Sedimentation rates. Similar to the Maastrichtian, the calculated thicknesses of the Paleocene succession have a good match with the measured thicknesses. In contrast to the high sedimentation rates during the Maastrichtian, low sedimentation rates prevailed during the Paleocene. Again, stratigraphic gaps in the basin were not reproducible with the constant sedimentation rates of the computer model.

4.4.2.2. Slope architecture. For the Paleocene, a distally steepened ramp was proposed (Kuss et al., 2000) contrasting with the rimmed platform of the upper Cretaceous with angles of 8°. The slope angle for the distally steepened ramp should be a little higher than 1° as homoclinal ramps normally exhibit slope angles of less than 1° (Ahr, 1973) or even less than 0.1° (Wright and Burchette, 1998). For the simulation of the sedimentary processes of the Paleocene only a relatively high slope angle of 6° reproduces the measured

sediment thicknesses. Simulations with lower slope angles shed more sediments into the basin because they reach their stability threshold during a shorter time span and cannot accumulate large quantities of sediment. Consequently, the sections of the platform–basin transect would have had similar thicknesses. But this was not observed in the field. So, at least for the Lower Paleocene a rimmed platform architecture is still valid.

4.4.2.3. Lithology. The phosphatic marls of the Lower Paleocene in section St. Anthony 1 and the hemipelagic shales of the Dakhla Formation at sections St. Paul 9, Bir Dakhli 2+3 and Wadi Tarfa1+2 are simulated as bioclastic fine wackestones and mudstones which resemble the lithology quite well.

4.4.2.4. Palaeowater depth. The benthic foraminiferal assemblages found in the sediments of section St. Paul, located at 32 km, were deposited during the Paleocene at palaeowater depths between 400 and 600 m, which is in the range of the simulated palaeowater depth of 400 m.

4.5. Benefits from stratigraphic modelling

The main reason for using stratigraphic modelling for this particular setting was the absence of the carbonate platform interior due to late Palaeogene and Neogene erosion. The computer simulation allowed to reconstruct the carbonate platform mainly based on slope sediments. Otherwise this would have been impossible. Furthermore, the stratigraphic modelling allows to evaluate some of the parameters and processes that are responsible for the growth of this particular carbonate platform.

The most important parameters that control the stratigraphic geometry of the platform in the Galala Mountains are changes in relative sea level, the sediment flux and the initial slope topography. The computer model proposed a mixed siliciclastic–carbonate platform with thicknesses of more than 200 m for the Maastrichtian and a carbonate platform with thicknesses of less than 70 m for the Danian–Selandian, both are completely eroded (today's Wadi Araba). The simu-

lated geologic parameters lithology, overall thickness and palaeowater depth are good matches with field and laboratory measurements of the individual sections.

Stratigraphic modelling is also an independent tool for calculating the angle of repose of slope sediments. The results of the Maastrichtian palaeoslope were compared with those of [Scheibner et al. \(2001b\)](#) which were confirmed by the computer model. Furthermore, the angle of repose of the Danian–Selandian slope sediments could be determined more accurately. The timing of the earlier proposed transition from a Maastrichtian rimmed platform to a Paleocene distally steepened ramp can be improved. The rimmed platform persisted at least until the late Paleocene what is documented by high slope angles of 6°.

On the other hand, the irregular sedimentation rates and the stratigraphic gaps in the basin could not be modelled because constant sedimentation rates for the different individual settings were assumed.

5. Conclusions

The two stratigraphic simulations of the Maastrichtian and the Danian–Selandian sediments of the Galala Mountains in the Eastern Desert of Egypt were conducted with the stratigraphic forward modelling program PHIL. These simulations allow the evaluation of some of the parameters that are responsible for the growth of the carbonate platform in the Galala Mountains and to compare these results with previously published data. Especially the angle of repose of the Danian to Selandian sediments could be determined more accurately. However, not all parameters could be modelled satisfactorily and therefore the modelling program is in our opinion best used for clarifying and visualizing the processes that are responsible for the evolution of the carbonate platform.

Acknowledgements

A.M. Bassiouni (Ain Shams University) is espe-

cially thanked for extensive logistic support. A.M. Morsi (Ain Shams University) is thanked for the open way in which he helped with all the problems we encountered during our stays in Egypt. Thanks are due also to T. Wagner (Bremen), C.G.St.C. Kendall, F. van Buchem, and J.P. Masse for their reviews and suggestions for improving the manuscript. The investigations were funded by the Graduiertenkolleg 'Stoff-Flüsse in marinen Geosystemen' of the University of Bremen and the German Science Foundation (DFG).

References

- Abdel-Kireem, M.R., Abdou, H.F., 1979. Upper Cretaceous–Lower Tertiary planktonic foraminifera from South Galala Plateau, Eastern Desert, Egypt. *Rev. Esp. de Micropal.* 11, 175–222.
- Ahr, W.M., 1973. The carbonate ramp: An alternative to the shelf model. *Trans. Gulf Coast Assoc. Geol. Soc.* 23, 221–225.
- Alegret, L., Thomas, E., 2001. Upper Cretaceous and lower Paleogene benthic foraminifera from northeastern Mexico. *Micropaleontology* 47, 296–316.
- Aubry, M.P., 1995. Towards an upper Paleocene–lower Eocene high resolution stratigraphy based on calcareous nanofossil stratigraphy. *Isr. J. Earth Sci.* 44, 239–253.
- Bandel, K., Kuss, J., 1987. Depositional environment of the pre-rift sediments – Galala Heights (Gulf of Suez, Egypt). *Berl. geowissensch. Abh. A* 78, 1–48.
- Berggren, W.A., Kent, D.V., Swisher, C.C. III, Aubry, M.P., 1995. A revised Cenozoic geochronology and chronostratigraphy. In: Berggren, W.A., Kent, D.V., Aubry, M.P., Hardenbol, J. (Eds.), *Geochronology, Time Scales, and Global Stratigraphic Correlation*. SEPM Spec. Publ. 54, Tulsa, pp. 129–212.
- Bowman, S.A., Vail, P.R., 1999. Interpreting the stratigraphy of the Baltimore Canyon section, offshore New Jersey with *Phil*, a stratigraphic simulator. In: Harbaugh, J.W., Watney, W.L., Rankey, E.C., Slingerland, R., Goldstein, R.H., Franseen, E.K. (Eds.), *Numerical experiments in stratigraphy: Recent advances in stratigraphic and sedimentologic computer simulations*. SEPM Spec. Publ. 62, Tulsa, pp. 117–138.
- Burchette, T.P., Wright, V.P., 1992. Carbonate ramp depositional systems. *Sediment. Geol.* 79, 3–57.
- Caron, M., 1985. Cretaceous planktic foraminifera. In: Bolli, H.M., Saunders, J.B., Perch-Nielsen, K. (Eds.), *Plankton Stratigraphy*. Cambridge University Press, Cambridge, pp. 17–86.
- Cortes, J., Risk, M.J., 1985. A reef under siltation stress: Cahuita, Costa Rica. *Bull. Mar. Sci.* 36, 339–356.
- Culver, S.J., 1993. Foraminifera. In: Lipps, J.H. (Ed.), *Fossil Prokaryotes and Protists*. Blackwell, Oxford, pp. 203–247.
- Emery, D., Myers, K.J., 1996. *Sequence Stratigraphy*. Blackwell, Oxford.
- Enos, P., 1991. Sedimentary parameters for computer modeling. In: Franseen, E.K., Watney, W.L., Kendall, C.G.S.C., Ross, W. (Eds.), *Sedimentary Modeling: Computer Simulations and Methods for Improved Parameter Definition*. Kansas Geological Survey, Lawrence, pp. 63–99.
- Faris, M., 1995. Late Cretaceous and Paleocene calcareous nanofossil biostratigraphy at St. Paul section, Southern Galala Plateau, Egypt. *Ann. Geol. Surv. Egypt* 20, 527–538.
- Franseen, E.K., Watney, W.L., Kendall, C.G.S.C., Rose, W., 1991. *Sedimentary Modeling: Computer Simulations and Methods for Improved Parameter Definition*. Kansas Geological Survey, Lawrence.
- Gietl, R., 1998. Biostratigraphie und Sedimentationsmuster einer nordostägyptischen Karbonatrampe unter Berücksichtigung der Alveolinen-Faunen. *Berichte aus dem Fachbereich Geowissenschaften der Universität Bremen* 112.
- Harbaugh, J.W., Watney, W.L., Rankey, E.C., Slingerland, R., Goldstein, R.H., Franseen, E.K., 1999. *Numerical Experiments in Stratigraphy: Recent Advances in Stratigraphic and Sedimentologic Computer Simulation*. SEPM Spec. Publ. 62, Tulsa.
- Hardenbol, J., Thierry, H., Farley, M.B., Jacquin, T., De Graciansky, P., Vail, P.R., 1998. Mesozoic and Cenozoic sequence chronostratigraphic framework of European basins. In: de Graciansky, P.C., Hardenbol, J., Jacquin, T., Vail, P.R. (Eds.), *Mesozoic and Cenozoic Sequence Stratigraphy of European Basins*. SEPM Spec. Publ. 60, Tulsa, pp. 3–13.
- Krenkel, E. (1925) *Geologie Afrikas*. Bornträger, Berlin.
- Kulbrok, F., 1996. Biostratigraphie, Fazies und Sequenzstratigraphie einer Karbonatrampe in den Schichten der Oberkreide und des Alttertiärs Nordost-Ägyptens (Eastern Desert, N'Golf von Suez, Sinai). *Berichte aus dem Fachbereich Geowissenschaften der Universität Bremen* 81.
- Kuss, J., 1986. Facies development of Upper Cretaceous–Lower Tertiary sediments from the monastery of St. Anthony/Eastern Desert, Egypt. *Facies* 15, 177–194.
- Kuss, J., Leppig, U., 1989. The early Tertiary (middle–late Paleocene) limestones from the western Gulf of Suez, Egypt. *Neues Jahrb. Geol. Paläontol. Abh.* 177, 289–332.
- Kuss, J., Scheibner, C., Gietl, R., 2000. Carbonate Platform to Basin Transition along an Upper Cretaceous to Lower Tertiary Syrian Arc Uplift, Galala Plateaus, Eastern Desert. *Egypt. GeoArabia* 5, 405–424.
- LeRoy, L.W., 1953. Biostratigraphy of the Maqfi Section, Egypt. *Geol. Soc. Am. Mem.* 54.
- Leyrer, K., Strohmenger, C., Rockenbauch, K., Bechstaedt, T., 1999. High-resolution forward stratigraphic modeling of Ca₂-carbonate platforms and off-platform highs (Upper Permian, Northern Germany). In: Harff, J., Lemke, W., Stattegger, K. (Eds.), *Computerized Modeling of Sedimentary Systems*. Springer, Berlin, pp. 307–339.
- Luger, P., 1985. Stratigraphie der marinen Oberkreide und des

- Alttertiärs im südwestlichen Obnubien-Becken (SW-Ägypten) unter besonderer Berücksichtigung der Mikropaläontologie, Palökologie und Paläogeographie. Berl. Geowiss. Abh. A (Geol. Paläontol.) 63.
- Lüning, S., Marzouk, A.M., Kuss, J., 1998. The Paleocene of central East Sinai, Egypt: 'Sequence stratigraphy' in monotonous hemipelagites. *J. Foraminif. Res.* 28, 19–39.
- Marco Polo Software Inc., 1995. PHIL[®] 1.5 Manual. Houston.
- Martini, E., 1971. Standard Tertiary and Quaternary calcareous nannoplankton zonation. In: Farinacci, A. (Ed.), Proceedings of the Second Planktonic Conference, Roma 1970, Tecnoscienza, pp. 739–785.
- Marzouk, A.M., Scheibner, C., in press. Calcareous nannofossil biostratigraphy and paleoenvironment of the late Cretaceous–Paleogene of the Galala Mountains, Eastern Desert, Egypt. Courier Forschungsinstitut Senckenberg.
- Miall, A.D., 1997. The Geology of Stratigraphic Sequences. Springer, Berlin.
- Mount, J.F., 1984. Mixing of siliciclastic and carbonate sediments in shallow shelf environments. *Geology* 12, 432–435.
- Moustafa, A.R., Khalil, M.H., 1995. Superposed deformation in the northern Suez Rift, Egypt: Relevance to hydrocarbons exploration. *J. Pet. Geol.* 18, 245–266.
- Norris, R.D., Kroon, D., Klaus, A., 1998. Explanatory notes. In: Proceedings of the Ocean Drilling Program. Ocean Drilling Program, Texas A&M University, College Station, TX, pp. 11–44.
- Perch-Nielsen, K., 1985. Mesozoic calcareous nannofossils. In: Bolli, H.M., Saunders, J.B., Perch-Nielsen, K. (Eds.), Plankton Stratigraphy. Cambridge University Press, Cambridge, pp. 329–426.
- Perlmutter, M.A., De Boer, P.L., Syvitski, J.R.L., 1999. Geological observations and parameterizations. In: Harbaugh, J.W., Watney, W.L., Rankey, E.C., Slingerland, R., Goldstein, R.H., Franseen, E.K. (Eds.), Numerical Experiments in Stratigraphy: Recent Advances in Stratigraphic and Sedimentologic Computer Simulation. SEPM Spec. Publ. 62, Tulsa, pp. 25–28.
- Read, J.F., 1998. Phanerozoic carbonate ramps from greenhouse, transitional and ice-house worlds: Clues from field and modelling studies. In: Wright, V.P., Burchette, T.P. (Eds.), Carbonate Ramps. Geological Society, London, pp. 107–135.
- Reiss, Z., 1952. On the upper Cretaceous and lower Tertiary microfaunas of Israel. *Res. Counc. Isr. Bull.* 2, 37–50.
- Said, R., Kenawy, A., 1956. Upper Cretaceous and lower Tertiary foraminifera from northern Sinai, Egypt. *Micropaleontology* 2, 105–173.
- Said, R., 1962. The Geology of Egypt. Elsevier, Amsterdam.
- Scheibner, C., Kuss, J., Marzouk, A.M., 2000. Slope sediments of a Paleocene ramp-to-basin transition in NE Egypt. *Int. J. Earth Sci.* 88, 708–724.
- Scheibner, C., Marzouk, A.M., Kuss, J., 2001a. Maastrichtian–Early Eocene litho-biostratigraphy and Palaeogeography of the northern Gulf of Suez region, Egypt. *J. Afr. Earth Sci.* 32, 223–255.
- Scheibner, C., Marzouk, A.M., Kuss, J., 2001b. Shelf architectures of an isolated Late Cretaceous carbonate platform margin, Galala Mountains (Eastern Desert, Egypt). *Sediment. Geol.* 145, 23–43.
- Scheibner, C., Reijmer, J.J.G., Marzouk, A.M., Speijer, R.P., Kuss, J. (in press). From platform to basin: The evolution of a Paleocene carbonate Margin (Eastern Desert, Egypt). *Int. J. Earth Sci.*
- Schnack, K., 2000. Biostratigraphie und fazielle Entwicklung in der Oberkreide und im Alttertiär im Bereich der Kharga Schwelle, Westliche Wüste, SW Ägypten. Berichte Fachbereich Geowissenschaften, Universität Bremen 151.
- Speijer, R.P., Van der Zwaan, G.J., 1996. Extinction and survivorship of southern Tethyan benthic foraminifera across the Cretaceous/Paleogene boundary. In: M.B. Hart (Ed.), Biotic Recovery from Mass Extinction Events. *Geol. Soc. London Spec. Publ.* 102, pp. 343–371.
- Speijer, R.P., Schmitz, B., 1998. A benthic foraminiferal record of Paleocene sea level and trophic/redox conditions at Gebel Aweina, Egypt. *Palaeogeogr. Palaeoclimatol. Palaeoecol.* 137, 79–101.
- Strougo, A., Haggag, M.A.Y., Luterbacher, H., 1992. The basal Paleocene '*Globigerina*' *eugubina* zone in the Eastern Desert (St. Paul's Monastery, South Galala), Egypt. *Neues Jahrb. Geol. Paläontol. Monatsh.* 1992, 97–101.
- Strougo, A., Faris, M., 1993. Paleocene–Eocene stratigraphy of Wadi El Dakhl, Southern Galala plateau. *Middle East Res. Cent., Ain Shams Univ., Earth Science Serv.* 7, 49–62.
- Van Morkhoven, F.P.C.M., Berggren, W.A., Edwards, A.S., 1986. Cenozoic Cosmopolitan Deep-Water Benthic Foraminifera. *Bull. Centr. Rech. Explor.-Prod. Elf-Aquitaine, Mem.* 11. Elf-Aquitaine, Pau.
- Watney, W.L., Rankey, E.C., Harbaugh, J., 1999. Perspectives on stratigraphic simulation models: Current approaches and future opportunities. In: Harbaugh, J.W., Watney, W.L., Rankey, E.C., Slingerland, R., Goldstein, R.H., Franseen, E.K. (Eds.), Numerical Experiments in Stratigraphy: Recent Advances in Stratigraphic and Sedimentologic Computer Simulation. SEPM Spec. Publ. 62, Tulsa, pp. 3–21.
- Widmark, J.G.V., 2000. Biogeography of terminal Cretaceous benthic foraminifera: Deep-water circulation and trophic gradients in the deep South Atlantic. *Cretac. Res.* 21, 367–379.
- Widmark, J.G.V., Speijer, R.P., 1997a. Benthic foraminiferal ecomarker species of the terminal Cretaceous (late Maastrichtian) deep-sea Tethys. *Mar. Micropaleontol.* 31, 135–155.
- Widmark, J.G.V., Speijer, R.P., 1997b. Benthic foraminiferal faunas and trophic regimes at the terminal Cretaceous Tethyan seafloor. *Palaios* 12, 354–371.
- Wright, V.P., Burchette, T.P., 1998. Carbonate ramps: An introduction. In: Wright, V.P., Burchette, T.P. (Eds.), Carbonate Ramps. *Geol. Soc. London, pp.* 1–5.